Ocean Modelling 29 (2009) 115–127

Contents lists available at ScienceDirect

Ocean Modelling

journal homepage: www.elsevier.com/locate/ocemod

Effect of the surface wind stress parameterization on the storm surge modeling

Il-Ju Moon [a,*], Jae-Il Kwon [b,*], Jong-Chan Lee [b], Jae-Seol Shim [b], Sok Kuh Kang [b], Im Sang Oh [c], Seok Jae Kwon [d]

[a] College of Ocean Science/Ocean and Environment Research Institute, Cheju National University, Ara 1 Dong, Jeju 690-756, Republic of Korea
[b] Korea Research and Development Institute, P.O. Box 29, Ansan 425-600, Republic of Korea
[c] Seoul National University, Gwanakro 599, Gwanak-Gu, Seoul 151-749, Republic of Korea
[d] National Oceanographic Research Institute, Seohaero 195, Jung-Gu, Incheon 400-800, Republic of Korea

ARTICLE INFO

Article history:
Received 5 October 2008
Received in revised form 22 March 2009
Accepted 24 March 2009
Available online 31 March 2009

Keywords:
Wind stress
Drag coefficient
Typhoon
Storm surge
Grid resolution

ABSTRACT

The wind stress over ocean is a crucial surface forcing in the storm surge modeling. This study investigates the effect of surface wind stress parameterizations and grid resolutions on the storm surge modeling. Three drag coefficient (C_d) formulas at high wind speeds have been tested for the Super Typhoon Maemi (2003) using the grid resolution of 1/12°, 1/60°, and 1/360°: (i) the linearly-increasing C_d by Wu [Wu, J., 1982. Wind-stress coefficients over sea surface from breeze to hurricane. J. Geophys. Res. 87, 9704–9706], (ii) the fast-increasing C_d by the WAVEWATCH III (WW3) model, and (iii) the leveling-off C_d by the coupled wind–wave (CWW) model. Experimental results show that a higher resolution model that has a better resolution of complex topography and the coastline produces higher surge, on the average. In particular, when the grid resolution of the storm surge model is greatly improved, the CWW model with the leveling-off C_d at high winds shows the best performance in the surge simulation, while both WW3 and Wu models with unrealistic high C_d at high winds tend to produce an overestimated surge.

1. Introduction

The air–sea momentum flux (or wind stress) over the ocean is a key surface forcing in the storm surge modeling and a crucial factor determining model performance (Doyle, 2002; Kim et al., 2008; Moon, 2005; Xie et al., 2008). It has long been recognized that the wind stress (or the drag coefficient C_d) depends on wind speed, as well as on the sea state and atmospheric stability (Monin and Obukhov, 1954; Charnock, 1955; Large and Pond, 1981; Smith et al., 1992). However, the bulk type formulas that are widely used in many storm surge models assume that the wind stress magnitude is a unique function of the wind speed, being independent of the sea state (Large and Pond, 1981). They are based on field measurements in weak to moderate wind regimes less than 25 m s $^{-1}$ and predict a monotonic increase of the C_d with wind speed.

A number of studies suggested that the sea states have a significant influence on the sea surface stress (Smith et al., 1992; Janssen, 1992; Mastenbroek et al., 1993). From measurements in the North Sea, Smith et al. (1992) found that the sea drag decreases as wave age increases. Janssen (1989, 1991, 1992) pointed out that wave-induced stress in young wind seas might be a substantial amount of the total stress in the surface layer, resulting in a considerable enhancement of the drag. Based on the theory of Janssen (1991), several studies on the coupling of surface waves and storm surges have been conducted using the wave-induced stress directly estimated from ocean wave models (Mastenbroek et al., 1993; Zhang and Li, 1997; Moon and Oh, 2003) and showed a significant increase of the C_d at high wind speeds. These results are also based on the field and laboratory measurements in the weaker wind regimes tend to be far from real storm wind magnitudes.

Recently, Powell et al. (2003) reported the drag coefficient derived from observed wind profiles using hundreds of GPS sondes launched from aircraft in tropical cyclones. These measurements were among the first estimates made in hurricane conditions with high wind speeds above 30 m s $^{-1}$. This study showed that the C_d in hurricane force conditions tends to level off or even decreases as the wind speed increases. A leveling-off C_d at high wind speeds was also found in laboratory experiments by Alamaro et al. (2002) and Donelan et al. (2004). Theoretically, Emanuel (2003) also predicted that the drag coefficient should be capped at a constant value at sufficiently high wind speeds based on the energy balance of a hurricane system. From numerical simulations for the idealized and real hurricanes, Moon et al. (2004b,c) also showed a reduced C_d at high wind speeds. These

* Corresponding authors. Tel.: +82 64 754 3412; fax: +82 64 756 3483 (I.-J. Moon), tel.: +82 31 400 6803; fax: +82 31 408 5827 (J.-I. Kwon).
E-mail addresses: ijmoon@cheju.ac.kr (I.-J. Moon), jikwon@kordi.re.kr (J.-I. Kwon).

1463-5003/$ - see front matter © 2009 Elsevier Ltd. All rights reserved.
doi:10.1016/j.ocemod.2009.03.006

results are quite different from those widely used in present storm surge models.

This clearly demonstrates that most storm surge models have overestimated surface wind stresses at high wind speeds. In particular, the wind stresses in coupled surge–wave models have been overestimated significantly since they predict an even faster increase of C_d at high wind speeds. However, it is surprising that models with unrealistic high C_d have produced reasonable or even better surge simulations (Mastenbroek et al., 1993; Zhang and Li, 1997). In this study, we will demonstrate that this is accomplished by compensating the surge errors due to the coarse grid resolution with excessively large surface wind stresses. Also we will show that using a high-resolution model and a reduced C_d at high wind speeds can yield a successful simulation of the storm surge in typhoon conditions.

This study aims to investigate impacts of the surface wind stress parameterization and the grid resolution on storm surge modeling with a special focus on the role of surface waves. For this purpose, three C_d parameterizations at high wind speeds are tested in the surge simulation for Super Typhoon Maemi (2003): (i) the linear relationship by Wu (1982), (ii) the fast-increased C_d by the WAVEWATCH III (WW3) model (Tolman, 2002), and (iii) the leveling-off C_d by Moon et al. (2004a). The latter is based on a coupled wave-wind (CWW) model and shows the most consistent result with recent field and laboratory measurements at high winds. Details of three surface stress parameterizations are described in Section 2. The impact of the grid resolution on the storm surge simulation is investigated using additional sensitivity experiments to three grid resolutions (1/12° × 1/12°, 1/60° × 1/60°, and 1/360° × 1/360°).

Effects of surface waves on wind stress can be summarized by two factors (Moon et al., 2004b,c): (i) the reduced magnitude of the C_d at high winds and (ii) the asymmetric C_d distributions relative to the storm center due to asymmetric wave fields. When typhoons move with a translation speed comparable to the group speed of dominant waves, waves to the right of the typhoon track are exposed to prolonged forcing from wind, i.e., they become "trapped" within the hurricane (resonance effect or dynamic fetch). This produces an asymmetric wave field relative to the storm center, which is totally different from wind fields (Moon et al., 2003a). The present study also focuses on investigating the role of surface waves on the C_d calculation and their resultant impacts on storm surge modeling.

In this study, accurate simulations of surface wind and wave fields are important prerequisites for successful experiments. Wind fields are calculated from the Primitive Vortex Model (PVM) and wave simulation is conducted with the CWW model (Moon et al., 2004a). Descriptions on the experimental design and the model configuration are given in Section 3. Section 4 introduces the wind and wave field specifications and validations for Typhoon Maemi. Section 5 describes experimental results for the response of the storm surge to the different surface wind stress parameterizations and grid resolutions. The summary and conclusions are given in the last section.

2. Wind stress parameterizations

This study investigates the effect of surface wind stress parameterizations on storm surge modeling. In this section, three types of wind stress formulas used in this study will be described. The first is a bulk type formula (hereafter, Wu) using a simple linear relationship between C_d and wind speed suggested by Wu (1982). The wind stress (τ) is expressed by

$$\tau = \rho_a C_d \cdot W^2, \tag{1}$$

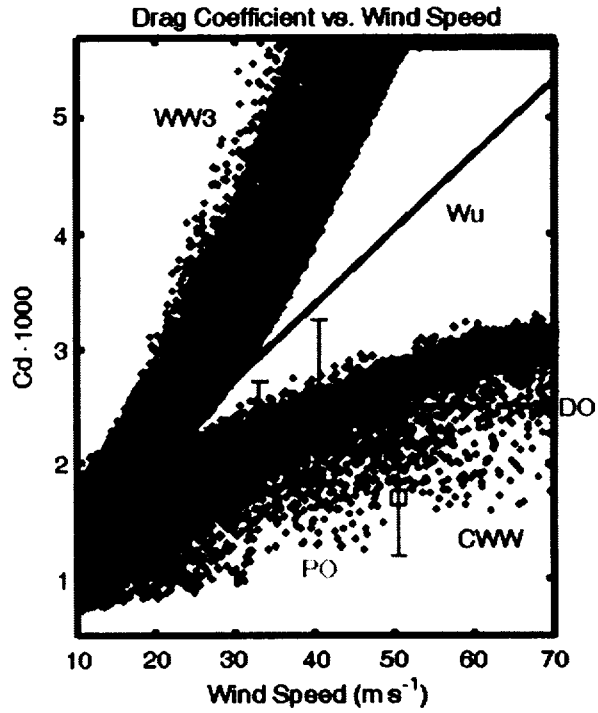

Fig. 1. A scatterplot of the C_d as a function of the wind speed at 10-m height obtained from WW3 (blue dots), CWW (black dots) and Wu (red line) parameterizations during the passage of Maemi. Model outputs of 6-h interval at all grid points are used for the scatterplot. A dashed line (DO) represents the C_d based on Donelan et al. (2004). Symbols (□) represent the C_d estimated from GPS sonde data in various hurricanes (Powell et al., 2003). Vertical bars (PO) represent the range of estimates based on 95% confidence.

$$C_d = 0.8 + 0.065 \cdot W, \tag{2}$$

where ρ_a is the air density and W is the wind speed (unit is m s^{-1}).

The second is an internal C_d parameterization (hereafter, WW3) of the WAVEWATCH III model based on Tolman and Chalikov (1996). The C_d at a given reference height (here, 10 m above sea surface) is expressed as

$$C_d = 10^{-3}\left(0.021 + \frac{10.4}{R^{1.23} + 1.85}\right), \tag{3}$$

with

$$R = \ln\left(\frac{10g}{\chi\sqrt{\alpha}u_{e10}^2}\right), \tag{4}$$

where χ is a constant value (0.2), u_{e10} is an effective wind speed at 10-m height, and α is the nondimensional energy level at high frequencies, which is expressed in terms of the wave age (c_p/u^*),

$$\alpha = 0.57\left(\frac{c_p}{u_*}\right)^{-3/2} \tag{5}$$

Here, u^* is the friction velocity and c_p is the phase speed of the wave at the peak frequency. For fully grown seas this parameterization is

Table 1
Experiments investigating the effect of grid resolution on storm surge modeling.

Name	Resolution	Type of C_d
Exp. 1	1/12°	Wu (1982)
Exp. 2	1/60°	
Exp. 3	1/360° (~300 m)	

similar to the commonly used bulk parameterization with a constant Charnock coefficient. However, it yields higher drag for younger waves at any given wind speed, being consistent with the empirical parameterizations by Donelan (1990) and Drennan et al. (2003).

The third (hereafter, CWW) is based on a coupled wave–wind model (CWW) of Moon et al. (2004a,b). In the CWW model, the complete wave spectrum is first constructed by merging the WW3 spectrum in the resolved frequency range (vicinity of the spectral peak) with the spectral tail parameterization of Hara and Belcher (2002). The result is then incorporated into the wave boundary layer (WBL) model (Hara and Belcher, 2004) to explicitly calculate the wave-induced stress vector, the mean wind profile, and C_d over any given complex seas. The WBL model is based on the combination of momentum conservation and energy conservation inside the WBL and it obviates the need

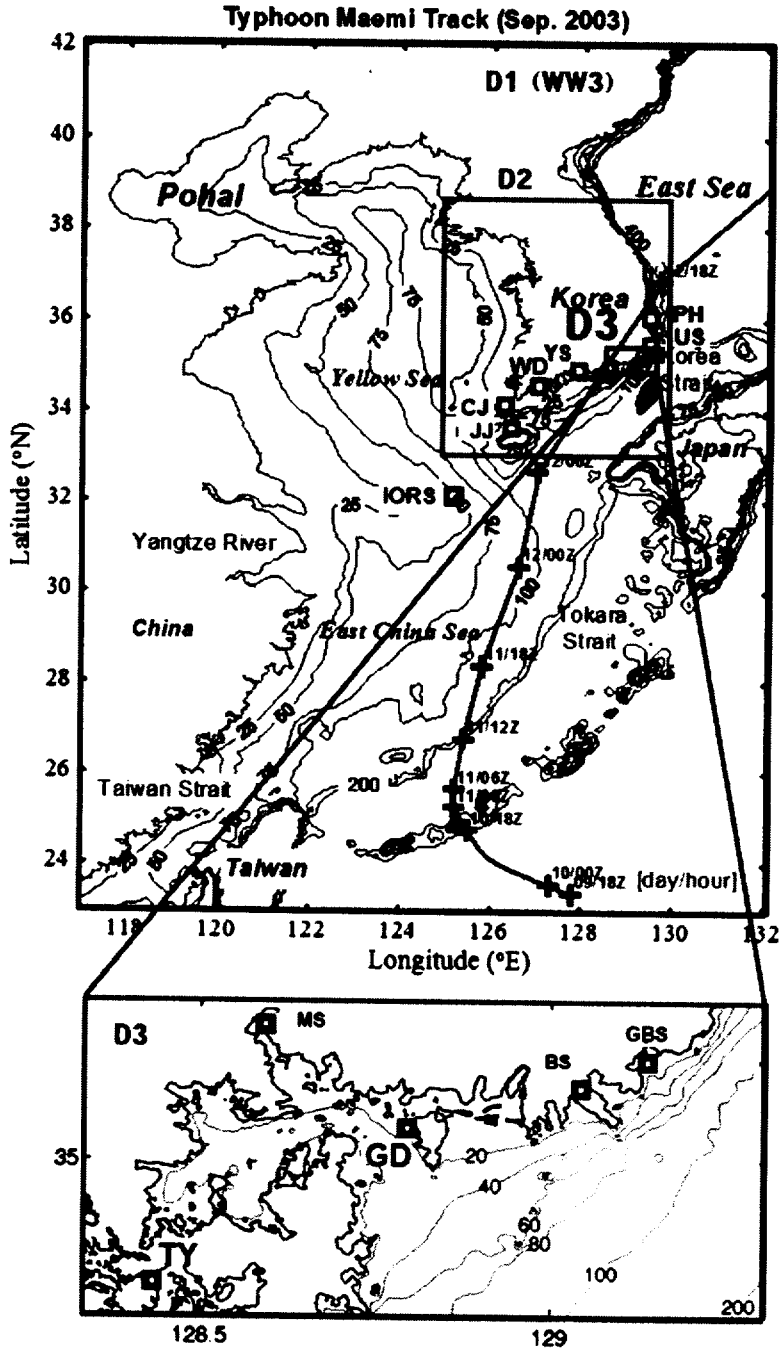

Fig. 2. Topography and domains for the storm surge model, the WW3 and CWW models with the track (red line) of Typhoon Maemi. Green boxes, D1, D2, and D3, represent domains of the storm surge model with the 1/12° × 1/12°, 1/60° × 1/60°, and 1/360° × 1/360° grid resolution, respectively. The WW3 and CWW models use D1 domain. Blue squares represent locations of observational stations (MS, Masan; BS, Busan; TY, Tongyoung; PH, Pohang; US, Ulsan; YS, Yeosu; WD, Wando; CJ, Chujado; JJ, Jeju; GD, Gadukdo; IORS, Ieodo ocean research station; GBS, Gwangan bridge station).

to introduce an empirical eddy viscosity parameterization (Hara and Belcher, 2004). Moon et al. (2004c) found that the neutral C_d levels off at high wind speeds under tropical cyclones, being consistent with recent observations. The most important finding of this study is that the sea drag is mainly determined by two parameters: the input wave age (wave age determined by the peak frequency of wind energy input) and the wind speed, regardless of the complexity of the wave field under a real hurricane, and that the drag increases with the input wave age at very high winds.

Fig. 1 compares three C_d scatterplots against wind speed for Typhoon Maemi. At moderate winds below 20 m s^{-1}, the three drag formulations show similar patterns. However, at high winds above 20 m s^{-1}, the CWW produces a much lower C_d, while the WW3 predicts a very high C_d. Results of the CWW are similar to those of Donelan et al. (2004) based on the wave tank experiments and within the error bars estimated by Powell et al.'s (2003) GPS sonde observations during hurricane conditions. The linear relationship of Wu (red line), which is widely used in storm surge models, lies between the two models. An interesting point is that the WW3 sets an upper limit of C_d for the model stability. This fact further suggests that the WW3 overestimates C_d at high winds unrealistically (Moon et al., 2007, 2008).

Table 2
Experiments investigating the effect of wind stress parameterization on storm surge modeling.

Name	Resolution	Type of C_d
Exp. 4	1/12°	WW3
Exp. 5	1/60°	
Exp. 6	1/360° (~300 m)	
Exp. 7	1/12°	CWW
Exp. 8	1/60°	
Exp. 9	1/360° (~300 m)	

3. Experimental designs and model configurations

3.1. Experimental designs

In order to accomplish the aims of the present study as described in Section 1, two types of numerical experiments are designed. The first experiment is to investigate the effect of the grid resolution on the storm surge model (Table 1). For this experiment, 3-step nesting grids are introduced. The first domain (D1) covers the entire Yellow and East China Seas with the 1/12° × 1/12° grid resolution (see Fig. 2). The second domain (D2) covers 33°N–39°N, 125°E–130°E with the 1/60° × 1/60° grid resolution. The D1 and D2 domains adapt a spherical coordinate system. The third domain (D3), where 3 tidal stations (Tongyoung, Masan, and Busan) were included, was discretized with the 300 m × 300 m (about 1/360° × 1/360°) grid resolution under a Cartesian coordinate system. Exp. 1 adapts a coarse resolution grid using only D1 domain, while Exp. 2 and 3 adapt finer resolution grids using the nested domains, D2 and D3, respectively. In these experiments, the linear C_d relationship of Wu (1982) is used for the surface wind stress calculation. The sensitivity of the grid resolution to storm surge modeling has been investigated by comparing the computed sea levels with observations at 9 tidal stations along the Korean coasts (see Fig. 2). Here it shoud be noticed that the finest domain (D3) covers only a small area and so comparisons in Exp. 3 are only made at three stations (Busan, Masan, and Tongyoung). The second experiment is designed to investigate the effect of wind stress parameterizations on the storm surge modeling (Table 2). For this experi-

Table 3
Best track, central pressure, and maximum wind speed of Typhoon Maemi.

Time in UTC (yyyymmddhh)	Latitude (°N)	Longitude (°E)	Pressure (hPa)	Wind (m s^{-1})
2003090800	19.7	133.9	980	28.3
2003090806	20.0	132.8	975	30.9
2003090812	20.4	132.0	975	30.9
2003090818	21.0	131.2	970	33.5
2003090900	22.0	130.4	960	36.0
2003090906	22.6	129.4	950	41.2
2003090912	22.9	128.7	940	43.8
2003090918	23.3	127.8	930	46.3
2003091000	23.6	127.2	925	48.9
2003091003	23.7	126.9	920	48.9
2003091006	24.0	126.6	910	51.5
2003091009	24.2	126.3	910	51.5
2003091012	24.3	126.0	910	54.1
2003091015	24.6	125.7	910	54.1
2003091018	24.7	125.4	910	54.1
2003091019	24.8	125.4	910	54.1
2003091021	25.0	125.3	910	54.1
2003091100	25.2	125.1	910	54.1
2003091103	25.5	125.2	920	48.9
2003091106	25.9	125.3	920	48.9
2003091109	26.3	125.4	925	48.9
2003091112	27.0	125.6	930	48.9
2003091115	27.8	125.7	935	46.3
2003091118	28.4	125.8	935	46.3
2003091121	29.5	126.1	935	46.3
2003091200	30.5	126.5	930	48.9
2003091206	32.7	127.1	935	46.3
2003091209	33.9	127.5	945	41.2
2003091212	34.9	128.3	955	38.6
2003091218	37.0	129.8	970	30.9
2003091300	39.1	131.8	975	28.3

ment, two additional wind stress parameterizations, the CWW and WW3, are tested for the grid resolution of 1/12°, 1/60° and 1/360°, respectively.

3.2. The model description

In the surge simulation for Typhoon Maemi, the wind stress is calculated from the CWW, WW3, and wind model every 1-h interval and transferred to the storm surge model. The CWW model consists of the WW3, WBL, and the spectrum tail model (Moon et al., 2004a). The WW3 is a third-generation surface wave model that has been extensively validated for global and regional wave forecasts (Tolman 2002; Tolman et al., 2005). The present version of the WW3 has a regularly spaced longitude-latitude grid of 1/12° × 1/12° resolution, extending from 22°N to 42°N and from 117°E to 132°E. The minimum model depth is allowed to be 5 m and the time step is 900 s. The wave spectrum is discretized using 24 directions ($\Delta\theta = 15°$) and 40 frequencies extending from 0.02851 to 1.1726 Hz with a logarithmic increment $f_{n+1} = 1.1f_n$, where f_n is the n-th frequency.

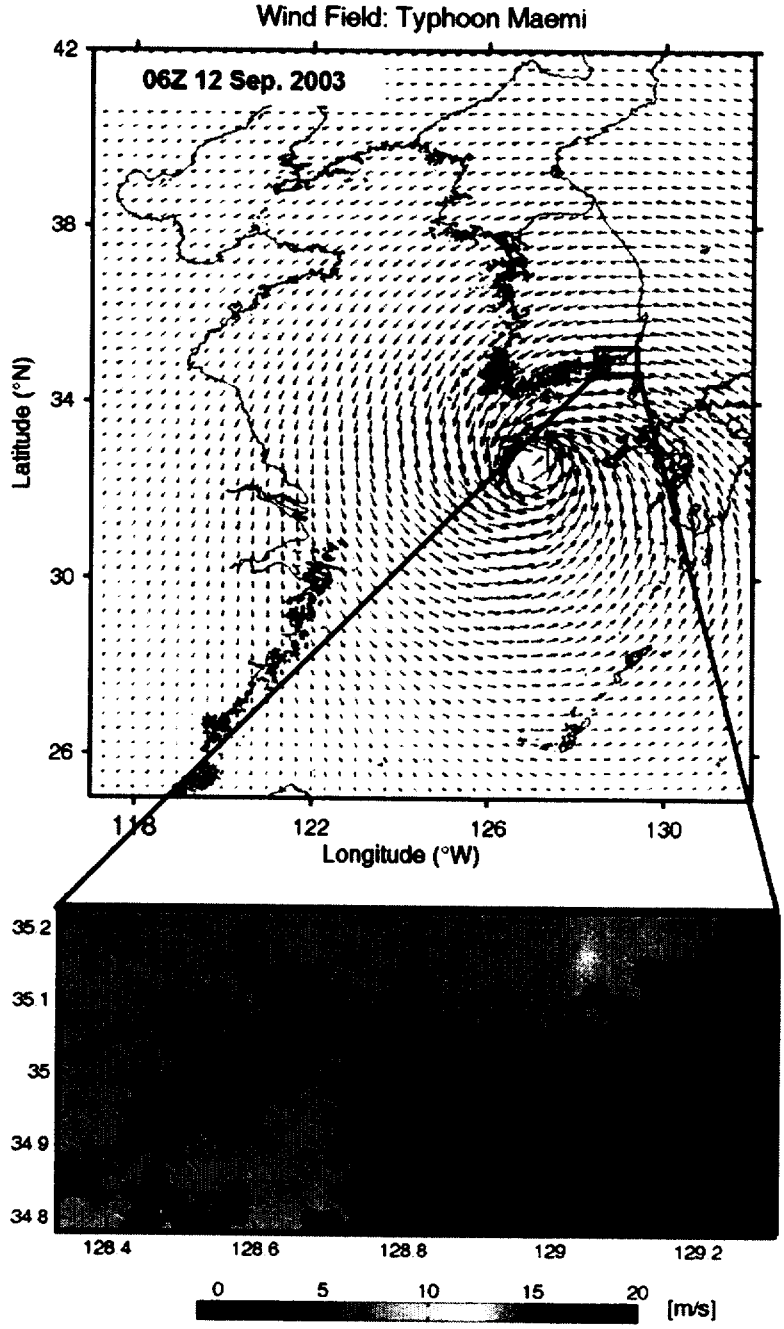

Fig. 3. Wind vector fields of Typhoon Maemi computed from the PVM at 06Z 12 September, 2003. Lower panel represents wind vectors (arrows) and speeds (color) for the nested domain (D3) with the 1/360° × 1/360° grid resolution.

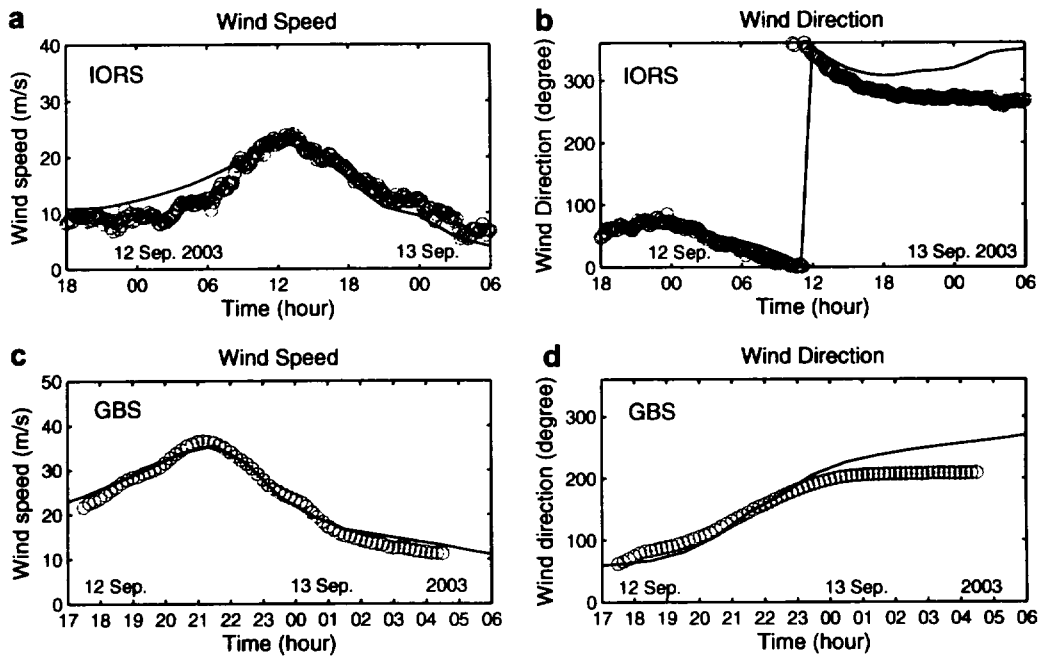

Fig. 4. Comparisons of wind speed (a and c) and wind direction (b and d) between model and observation at the IORS (a and b) and GBS (c and d) during the passage of Typhoon Maemi. Open circles and solid lines represent observations and the PVM outputs, respectively.

Table 4
RMS errors for wind speed and direction between model and observations at IORS and GBS during the period of Typhoon Maemi.

Stations	RMS errors	
	Wind speed ($m\,s^{-1}$)	Wind direction (°)
IORS	2.5	35.8
GBS	1.4	26.6

The bathymetry of the model domain is shown in Fig. 2. Note that the model configurations in the original WW3 and the CWW are same except the formulations of the C_d calculation. The WW3 calculates the C_d using Eqs. (3)–(5), but the CWW uses the WBL model of Hara and Belcher (2004).

The present storm surge model, the Korean Ocean Research and Development Institute Surge (KORDI-S) model, is based on depth-averaged momentum equations and the continuity equation. In this model, a staggered grid (Arakawa C grid) system allowing second order accuracy in space and a fully-implicit scheme are implemented with a conjugate gradient method (Strikwerda, 1989) for a large sparse matrix solver. Horizontal advection terms were treated explicitly using the sum of two other second-order difference schemes (Stelling, 1984). A one-way multi-nesting scheme was used to resolve complex coastal topography and uncertain open boundary conditions in higher-resolution grids. Sea surface elevations along open boundaries in the D1 domain were specified using an inverse barometric pressure. In this study, tidal influences on the storm surge simulation are not considered. This is because numerical experiments with tidal forcing using M2, S2, K1 and O1 constituents showed that the tidal effect on the surge simulation along the southern coasts of Korea, where tidal ranges are relatively small compared to the western coasts, was not significant (Lee et al., 2008). The open boundary for sea surface elevations in the D2 and D3 domains are specified by interpolating the sea surface elevations computed from the D1 domain spatially and temporarily. The wind stress input for the surge model is calculated from the three C_d parameterizations described in Section 2. The bottom stress (τ_b) is determined from a quadratic law and is given by

$$\tau_b = \rho_w C_f \sqrt{u_b^2 + v_b^2}, \tag{6}$$

where ρ_w is the sea water density, u_b and v_b are the bottom velocity components in the x- and y-directions, respectively, and C_f is an empirical coefficient for bottom friction. In this study, C_f was set to be 0.001 at depth <100 m and 0.0025 at depth $\geqslant$ 100 m.

3.3. Observation data

In order to verify wind inputs for the storm surge model, calculated from the PVM, we used time series of the wind speed and direction at Ieodo Ocean Research Station (IORS) and Gwangan Bride Station (GBS) (see Fig. 1). At the IORS, the mean wave parameters are also observed during the passage of Typhoon Maemi. These data, which constitute a unique data set observed in the open sea and near the typhoon's track, are used to investigate the performance of the wave model. Observed wave data at Gadukdo located in the shallow coastal sea are also used for the wave comparison (Fig. 1). Wind data at the IORS and GBS were adjusted to a height of 10 m using a logarithmic profile since they were obtained at 45-m and 50-m height, respectively. For the validation of the computed surge height, sea level data at 1-minute interval at 9 tidal stations (BS, TY, MS, PH, US, YS, WD, CJ, and JJ) along the Korean coasts are used (see Fig. 2). Here, the surge heights at each station have been averaged to hourly values after removing tidal components in order to remove high frequency signals and tides.

4. Typhoon Maemi wind and wave field specifications

4.1. Typhoon Maemi

Super Typhoon Maemi (2003) formed in the monsoon trough approximately 111 km east-southeast of Guam (JTWC, 2003). This cyclone tracked northwestward over Guam. Typhoon Maemi experienced rapid intensification beginning around 1800Z on 8 September due to enhanced upper level outflow and ocean warm eddy. This allowed the cyclone to reach super typhoon strength by 1200Z on 9 September and attain maximum intensity of 54 m s^{-1} 24 h later (Table 3). Typhoon Maemi made landfall at the Korean peninsula at around 1300Z on 12 September and, subsequently, tracking along the southeastern coast of Korea. Typhoon Maemi then moved into the East/Japan Sea and became an extratropical system at around 0600Z on 13 September.

One fatality was reported and a further 93 injuries occurred as Typhoon Maemi tracked over the islands of Miyakojima and Kumejima in the Okinawa prefecture, approximately 370 km southwest of Naha, Okinawa. These islands sustained property damage, flight cancellations and extensive loss of electricity. Peak sustained winds of 17 m s^{-1}gusting to 24 m s^{-1} were measured at Kadena Air Base. Southern Japan received significant precipitation and 48 people were evacuated from their homes in Nagasaki prefecture where landslides were reported. Typhoon Maemi was one of the most intense cyclones to strike Korea since 1950. Typhoon Maemi made landfall in Kosoung, Korea with an intensity of approximately 46 m s^{-1} and caused over 120 fatalities, with 1000s evacuated and approximately 4 billion dollars in damage reported. In Masan, residential and commercial areas located far from the Masan Port were flooded by the severe storm surge of about 2.1 m. Busan harbor also experienced tremendous damages at that time due to this record-breaking high surge height.

4.2. Wind and wave fields

In this study, the Primitive Vortex Model (PVM) was used to calculate the atmospheric pressure and sea surface wind fields for Typhoon Maemi. Unlike other simplified typhoon parameter models, the PVM includes an atmospheric boundary layer model including a primitive equation (Cardone et al., 1994). This model also introduces a multi-nesting grid system with three different grid resolutions and a moving coordinate system where inner nests move according to the center of typhoon. The PVM requires five input parameters such as the location and pressure of storm center, the radius of the maximum wind, and the background pressure and geostrophic wind fields. In this study these parameters were calculated using operational atmospheric model outputs of the Korea Meteorological Agency, satellite images, and synoptic surface data from ground stations from Korea, China, and Japan. Once all necessary parameters were acquired, the PVM calculates the sea surface pressure and wind fields at 1-hourly interval and passes them to the storm surge model. The performance of the PVM for 64 typhoons during 1979–1999 has been verified using measurements from buoys of the Japan Meteorological Agency and Kyusho ocean observation tower (Kang et al., 2002; Kwon et al., 2008). The results showed that the PVM simulates wind fields for various typhoons with high accuracy. Detailed descriptions and comparisons for the PVM are found in Kang et al. (2002).

Fig. 3 shows that wind vector fields computed from the PVM at 06Z 12 September 2003. The maximum wind speed reaches 45 m s^{-1} near the eye wall of the storm. During the passage of Typhoon Maemi, two marine stations at the coast and in the open sea, the GBS and IORS (see Fig. 2), observed the wind speed and direction and these data are compared with the PVM results (Fig. 4). The comparisons show that the PVM predicted the wind speed and direction at the coast and in the open seas during the Typhoon Maemi's period with a high accuracy. The root mean square (RMS) errors in the GBS and IORS are 1.4 m s^{-1} and 2.5, 1.4 m s^{-1} in wind speed, and 26.7° and 35.8° in direction, respectively (Table 4).

The verification of the computed surface waves is an important step before estimating the surface wind stress in the CWW model.

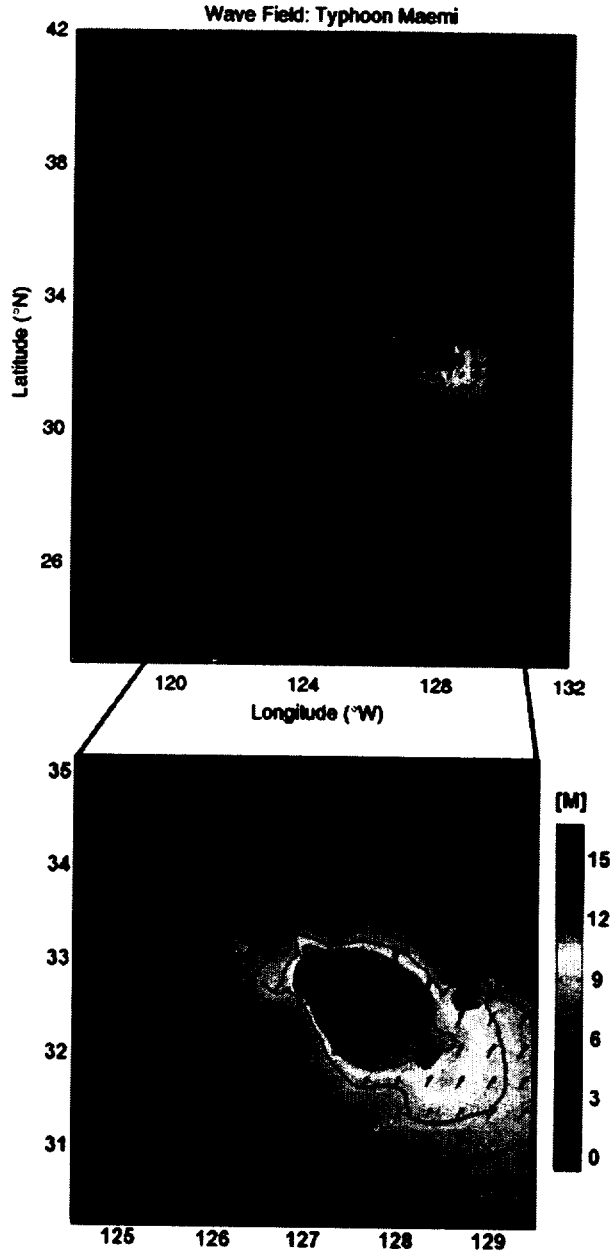

Fig. 5. Distribution of significant wave heights (contours), mean wave direction (arrows), mean wavelength (arrows) for Typhoon Maemi obtained by the wave model at 06Z 12 September, 2003. The arrow length is proportional to the mean wavelength. A solid line with asterisk is the storm track of 6-h interval.

This is because accurate stress calculations depend on accurate wave simulations. Fig. 5 shows distributions of the significant wave height (H_s, contours), the dominant wave direction (arrows), and the dominant wavelength (proportional to the arrow length) simulated by the CWW model during the period of Typhoon Maemi. The H_s reaches 16 m at 06Z 12 September. The maximum wave heights appear in the right forward quadrant of typhoon center. Fig. 6 compares the computed H_s, peak wave period, and mean

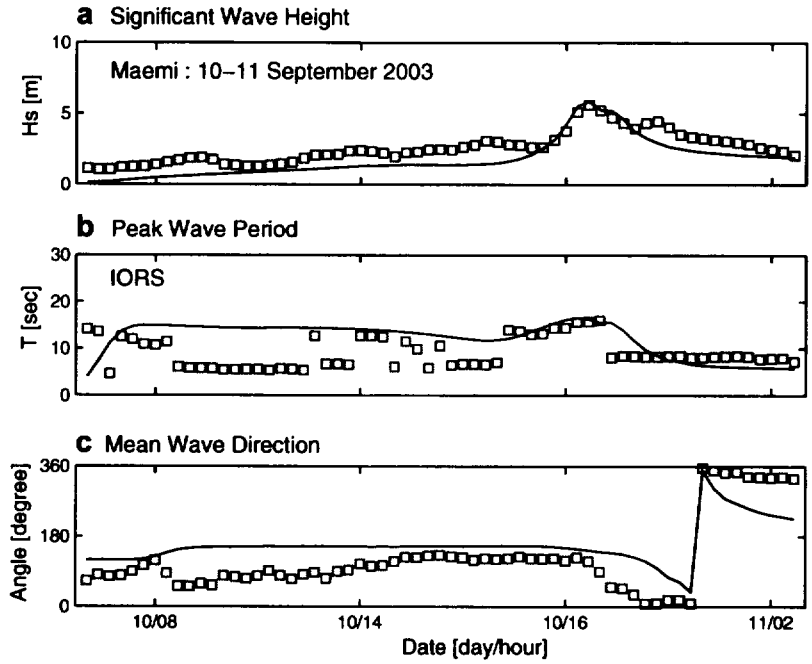

Fig. 6. Comparisons of (a) significant wave height, (b) peak wave period, and (c) mean wave direction between model outputs (solid lines) and measurements (squares) at the IORS during the passage of Typhoon Maemi.

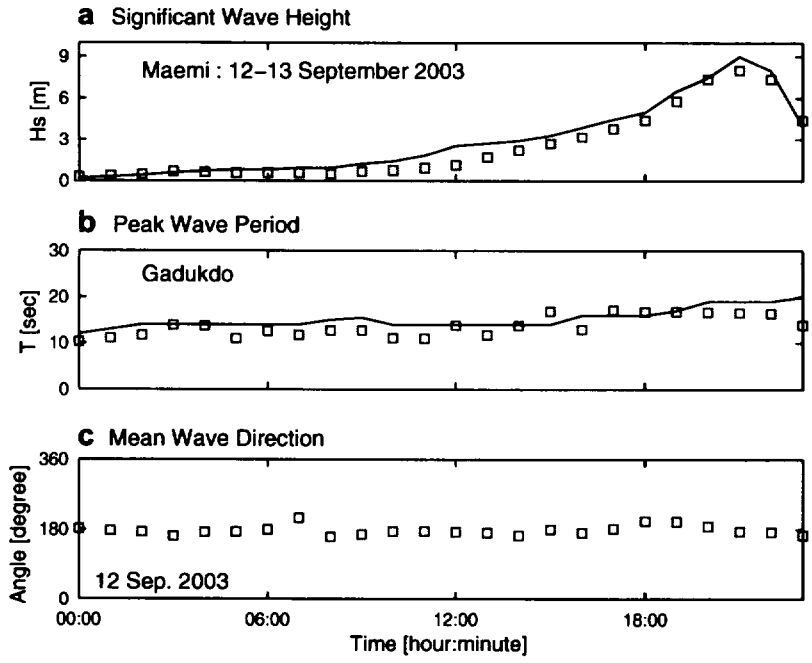

Fig. 7. As in Fig. 6, but at Gadukdo.

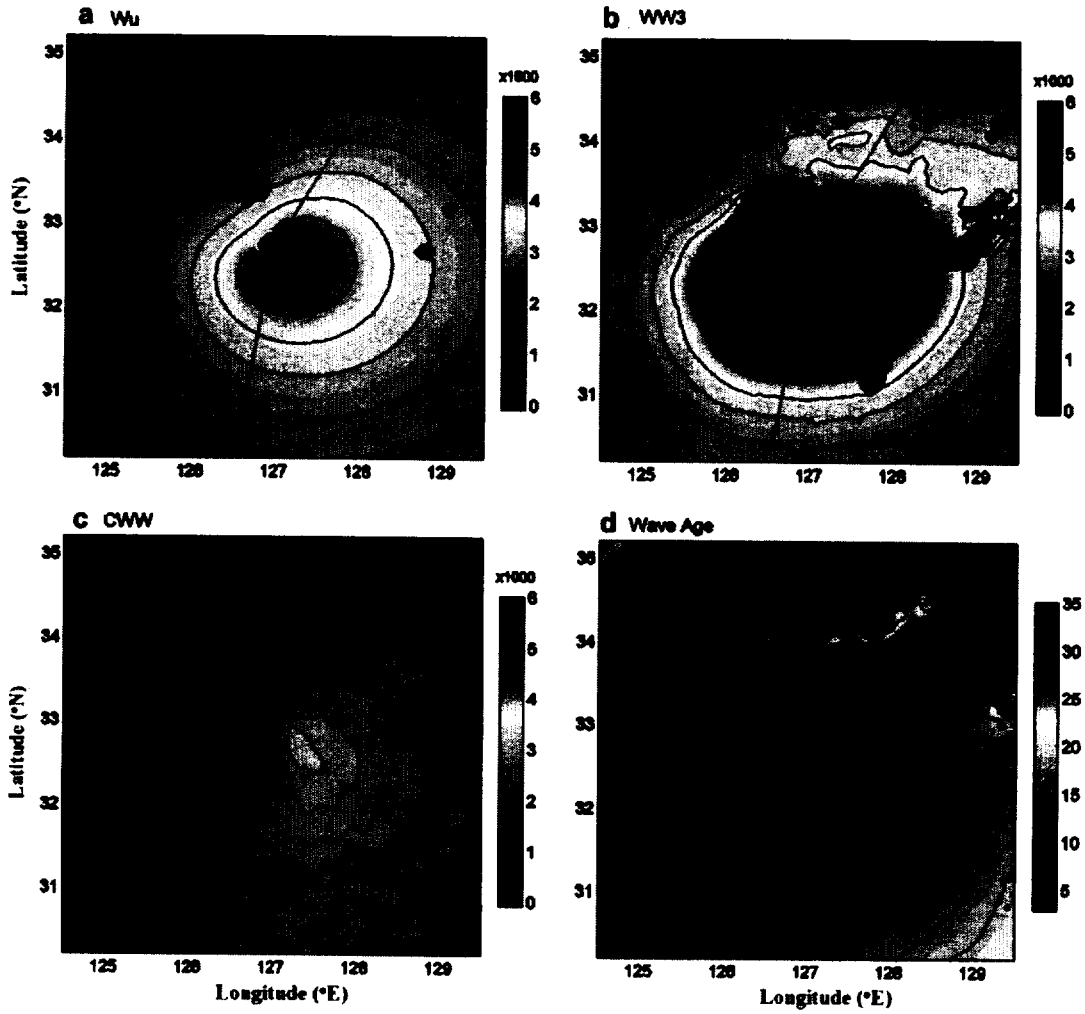

Fig. 8. Spatial distributions of the computed C_d using (a) Wu, (b) WW3, and (c) CWW parameterizations at 06Z 12 September, 2003. The wave age (d) is calculated from the CWW simulation.

wave direction with observations at the IORS. The maximum wave heights reach 6 m in both the observations and model. The computed wave heights, period, and direction are generally in good agreement with measurements throughout the passage of Typhoon Maemi. Since the IORS is located at the open ocean, further comparisons in the shallow coastal waters are presented in Fig. 7. Wave measurements at Gadukdo, where the water depth is about 14 m and the distance from the coast is about 300 m, recorded 8-m H_s at 20Z 12 September. The maximum is consistent with the CWW calculation, although the model results represent a slight overestimate.

5. Results and discussion

5.1. Neutral drag coefficients under Typhoon Maemi

In this section, we compare the computed C_d using the three stress parameterizations, Wu, WW3, and CWW. Fig. 8 represents the spatial distributions of the simulated C_d at 06Z 12 September 2003 for each parameterization. As suggested in Fig. 1, this clearly shows that not only their magnitudes, but also their spatial distributions, particularly in the positions of the maximum and minimum C_d in strong wind regimes, are very different. In the CWW model, the maximum C_d is found in the front right quadrant of the storm track and the minimum is found in the rear left quadrant, while the maximum (minimum) in the Wu formulation is found in the right (center) of the storm track. The former is very similar to the wave field (see Fig. 5) and the latter is identical to the wind field as expected. Under hurricane conditions, waves to the front right of the hurricane's track are usually exposed to prolonged forcing from wind, i.e., become "trapped" within the hurricane. The trapped waves produce higher, longer and older waves in the front right quadrant (Moon et al., 2003a). On the other hand, waves to the rear left of the track experience limited fetch and duration of wind forcing. These waves become lower, shorter, and younger. Moon et al. (2004b) predicted that higher, longer and more developed waves in the right front quadrant of the storm track produce higher sea drag; lower, shorter and younger waves in the rear left quadrant produce lower sea drag. This explains why locations of the maximum and minimum C_d in the CWW are different from those in the Wu formulation.

In Wu's parameterization, the maximum C_d is found to the right of the storm track, which is due to the asymmetric wind

distribution, where the maximum speed appears to the right of the forward storm direction. Usually, when a hurricane moves, actual wind speeds to the right (left) of its track become higher (lower) than those to the left (right) due to addition (subtraction) of the translation speed to the wind speed. In the WW3 result, the maximum C_d is found in areas along the eye wall. The C_d in the WW3 result is calculated using a function of the wave age (Eq. (5)) whereby the younger waves produce higher drag. Under typhoon conditions, waves usually experience a short fetch and duration due to the fast-varying wind characteristics in time and space, and consequently young waves become dominant (Fig. 8d). This explains why the C_d near the storm eye wall is very high. In Fig. 8b, the exact location of the maximum C_d is not clear because a maximum value (5.5×10^3) is constrained for the stability of the WW3 model internally.

Differences in the spatial distributions according to the C_d parameterizations also affect the total wind stress calculation and ultimately the surge simulation. However, it is difficult to distinguish the effects of the spatial distribution and the magnitude because the differences in the magnitude prevail as seen in Fig. 1. Comparisons of the surge simulation for the three C_d parameterizations will be presented in next section.

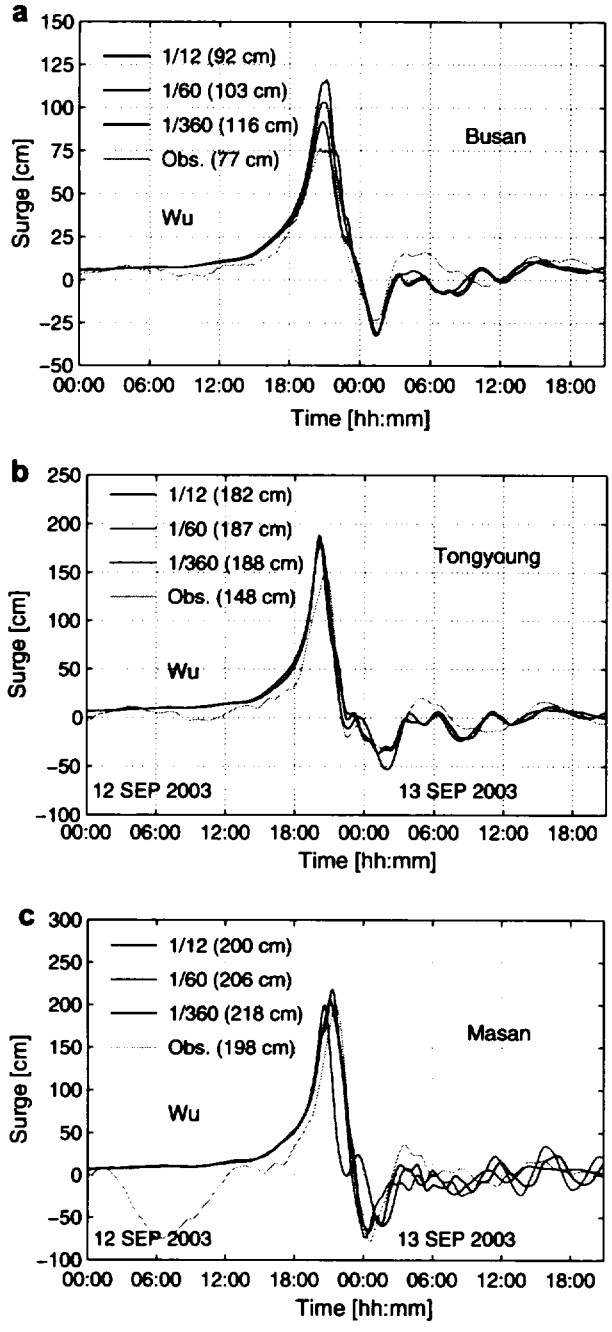

Fig. 9. Comparisons of the surge heights computed using the 1/12°, 1/60°, and 1/360° grid resolutions at (a) Busan, (b) Tongyoung, and (c) Masan during the passage of Maemi. In these experiments, the C_d formula of Wu (1982) has been used. The numbers in the brackets represent the peak surge for each case.

5.2. Effect of the grid resolution on the storm surge simulation

Three experiments were conducted to investigate the effect of the grid resolution on the storm surge modeling (Table 1). Here, all conditions for experiments are same except the grid resolution. The wind stresses are calculated using Wu's formula. Fig. 9 compares time series of the simulated surge heights for the 1/12°, 1/60°, and 1/360° gird resolutions at Busan, Tongyoung, and Masan where the large surge occurred during Typhoon Maemi. This shows that higher resolution models produce higher surges if other conditions are same. In particular at Busan, the 1/360° grid resolution produces about 24-cm higher surge than 1/12° does. The largest difference is mostly found during the peak of the surge.

In the model, the surge height is computed as the mean of the grid boxes. In a coarse grid, the box is large, which means that the surge height is averaged over a large area. Therefore, the peak surge averaged over a small area in a high-resolution model will be larger than that over a larger area in a low-resolution model. At complex coasts, in particular, the resolution effect will be more important because higher resolution grids better resolve the coastal geography, bathymetry and topography. When storms approach land, the water pileup and the resonant effects are major factors in producing a high storm surge in coastal areas (Moon et al., 2003b) and they are mostly determined by a coastal topography. If the coastal geometry has a complex shape, the water pileup and the resonant effects will play more important roles on the enhancement of the surge height.

The western and southern coasts of the Korea peninsula, where the largest surge events tends to occur, consist of many islands and bending coasts (see Fig. 2). Therefore, it is likely that a higher-resolution model that resolves a detailed, accurate topography and coastline tends to produce higher surges. Comparisons for six stations (Fig. 10) reveal that an overall 8.6-cm enhancement of the simulated surge has been made by introducing the improved grid resolution from 1/12° to 1/60°.

5.3. Effect of the wind stress parameterization on the storm surge simulation

Effects of the wind stress parameterization on the storm surge modeling have been investigated using an additional six experiments shown in Table 2. Here, three stress formulas from Wu, WW3, and CWW are applied for 1/60° and 1/360° grid resolutions during Typhoon Meami, respectively. From the comparison of spatial surge distributions for 1/360° resolution (see

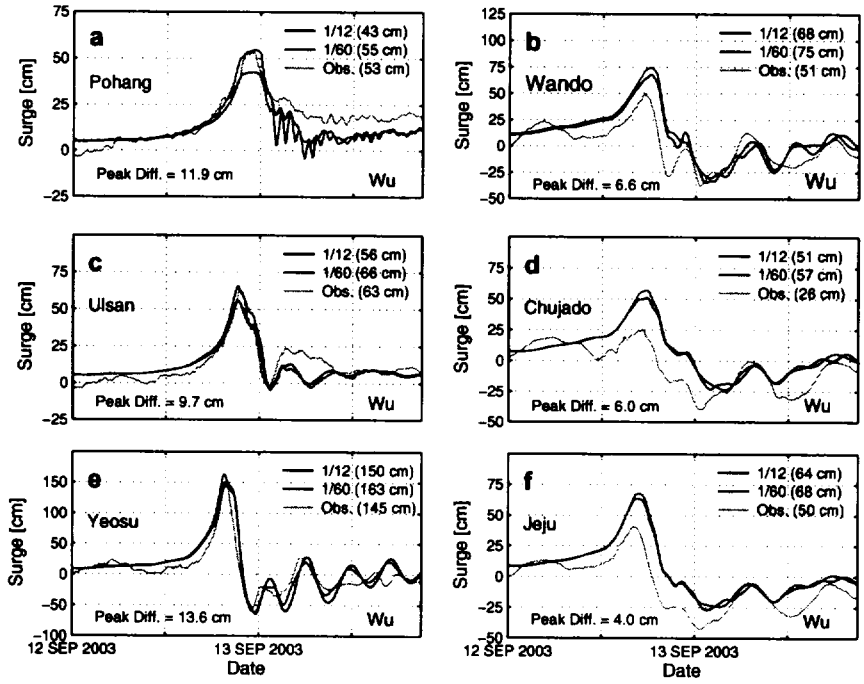

Fig. 10. Comparisons of the surge heights computed using the grid resolution of 1/12° and 1/60° at (a) Pohang, (b) Wando, (c) Ulsan, (d) Chujado, (e) Yeosu, and (f) Jeju during the passage of Maemi. In these experiments, the C_d formula of Wu (1982) has been used. The numbers in the brackets represent the peak surge for each case. Differences of the peak surge between1/12° and 1/60° are denoted at the bottom of each figure.

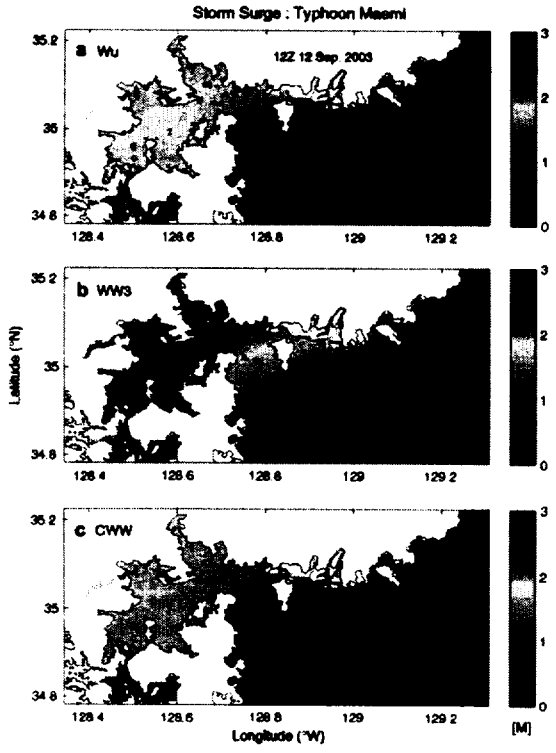

Fig. 11. Spatial distributions of the surge heights computed using the C_d formulas of (a) Wu, (b) WW3, and (c) CWW at 12Z 12 September 2003. In these experiments, the grid resolution of 1/360° has been used.

Fig. 11), it is found that the effect of the wind stress parameterization on the storm surge modeling is evident near the coastal areas. It shows that the model with the highest (lowest) C_d produces the highest (lowest) surge heights as expected. Fig. 12 compares time series of the simulated surge heights for Wu, WW3, and CWW at Busan, Tongyoung, and Masan according to the grid resolution. Comparisons between the simulated and observed peak surge values reveal that the WW3 formulation overestimates the surge peak of about 63 cm in Busan, 85 cm in Tongyoung, and 71 cm in Masan. Results by Wu also show a similar smaller overestimation. The CWW result shows the best performance in reproducing the observed peak surge at these stations (see Fig. 13a).

These results, however, depend strongly on the model grid resolution. From the RMS error analysis (Table 5 and Fig. 13b), it is found that the CWW formulation shows the best performance for the 1/360° resolution, while the WW3 result shows the worst result. For the coarse resolution (1/12°), the results are reversed. For the 1/60° resolution, the Wu result shows the best result. This demonstrates that, for both WW3 and Wu formulations, unrealistically-predicted high C_d at high wind speeds tends to produce the overestimated surge when the grid resolution is greatly improved. Therefore, it is likely that storm surge models with a coarse resolution (less than 1/12°) require a high C_d to compensate for the underestimated surge height due to the coarse resolution. Also, in many storm simulations the wind speed and the storm size tend to be under predicted, mainly due to insufficient spatial and temporal resolution in atmospheric models. Therefore, a large C_d tends to compensate for the wind error in the speed and size of the storm. These are possible reasons that many storm surge models use unrealistically high drag during strong wind conditions.

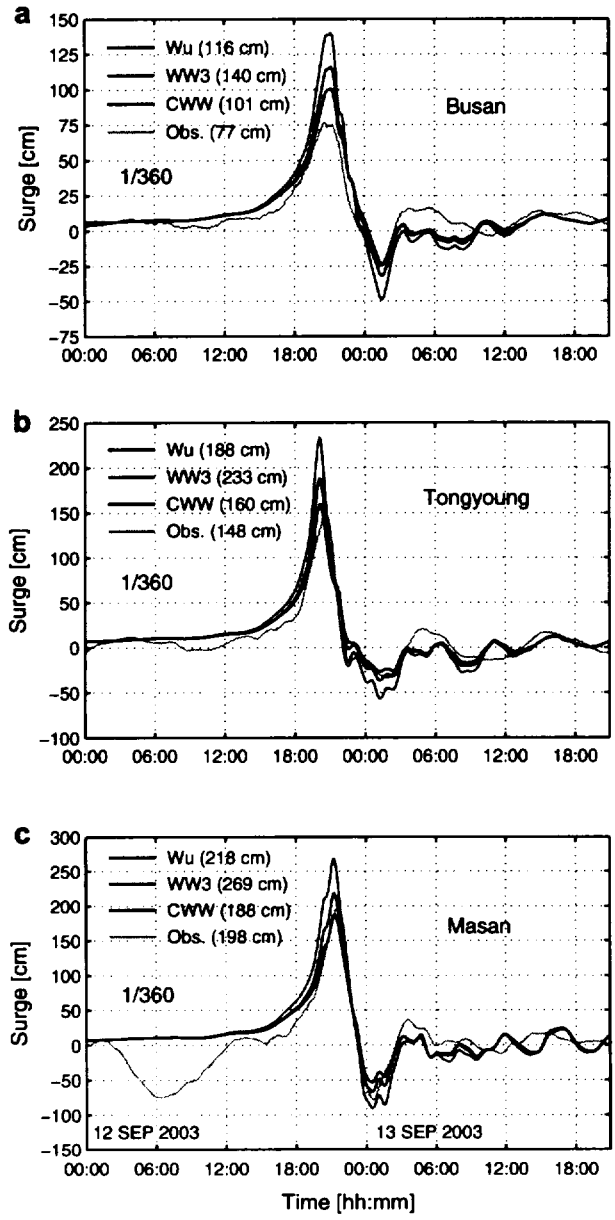

Fig. 12. Comparisons of the surge heights computed using the C_d formulas of Wu, WW3, and CWW at (a) Tongyoung (b) Busan, and (c) Masan during the passage of Maemi. In these experiments, the grid resolution of 1/360° has been used. The numbers in the brackets represent the peak surge for each case.

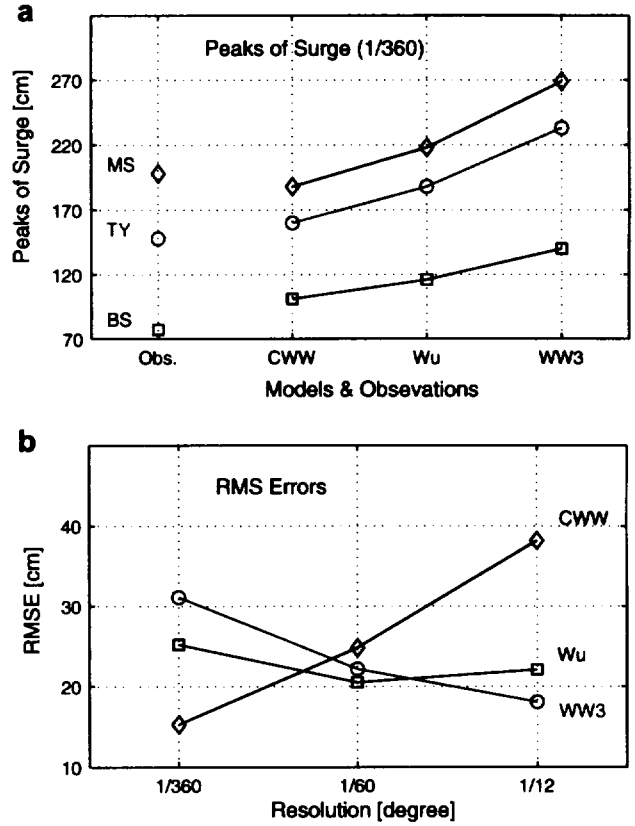

Fig. 13. (a) The peaks of the surge height at Busan, Tongyoung, and Masan and (b) RMS errors between models and observations during the period of Typhoon Maemi. The peaks of surge height are computed using the 1/360° grid resolution.

Table 5
RMS errors between models and observations for experiments of Tables 1 and 2. RMS errors for 1/12° and 1/60° grid resolution are calculated using 9 tidal stations (BS, TY, MS, PH, US, YS, WD, CJ, and JJ). Those for 1/360° are calculated using 3 tidal stations (BS, TY, and MS).

Grid resolution	RMS errors		
	WW3 (cm)	Wu (cm)	CWW (cm)
1/12°	18.1	22.1	38.2
1/60°	22.2	20.5	24.8
1/360°	31.1	25.2	15.3

6. Summary and conclusion

The air–sea momentum flux (or wind stress) over ocean is a major surface forcing which determines the performance of storm surge modeling. So far, most storm surge models have used a linearly (or even faster) increasing drag coefficient (C_d) as wind speed increases, resulting in very high C_d at high wind speeds. These trends are very different from those suggested by recent field, laboratory, theoretical, and numerical studies, showing a leveling-off (or even decreasing) C_d at high wind speeds. This study aims to investigate the effect of the C_d parameterizations and grid resolution on storm surge modeling for Typhoon Maemi.

A series of numerical experiments were conducted for three grid resolutions (1/12° × 1/12°, 1/60° × 1/60°, and 1/360° × 1/360°) using three C_d formulas: (i) the linearly-increasing C_d by Wu (1982), (ii) the fast-increasing C_d by the WAVEWATCH III (WW3) model, and (iii) the leveling-off C_d by the coupled wind–wave (CWW) model. The experimental results for Typhoon Maemi showed that the WW3 and Wu (1982) formulations produce very high C_d at high wind speeds above 30 m s^{-1}, while the CWW formulation produces a much lower C_d. It is found that C_d in the latter is the most consistent result with the recent field and laboratory measurements during high winds. The spatial distributions of the simulated C_d also showed very different according to the used parameterizations, particularly in the location of the C_d maximum and minimum.

In the experiments using different grid resolutions, a higher resolution model tended to produce higher surge if other conditions

are same. In particular at Busan, the 1/360° grid resolution model produced about 24-cm higher surge than the 1/12° does. This result is because a higher resolution surge model averages the surge height over a smaller area and the coastal geography and topography are better resolved, which enhances surge heights more effectively by the water pileup and resonant processes. At the southern and western coasts of the Korean peninsula consisting of many islands and bending coasts, it is expected that an improvement in the grid resolution will lead to a large increment in the simulated surge.

Effects of wind stress parameterizations on the storm surge modeling depend on the model resolution. For the finest resolution (1/360°), the CWW formulation shows the best performance, while the WW3 formulation shows the worst result. For the coarse resolution (1/12°), the results are reversed. This study demonstrates that the storm surge model with a coarse resolution (less than 1/12°) requires an unrealistic high C_d such as WW3 and Wu formulas to compensate for the underestimated surge height due to the coarse resolution. Also, it shows that the combination of a high-resolution storm surge model and the CWW parameterization may greatly improve the storm surge prediction in typhoon conditions.

In this study, however, only one specific storm surge model has been tested for Typhoon Maemi. Effects of the wind stress parameterizations and the grid resolution on the storm surge modeling may appear differently in other models and other typhoon cases. More experiments will be necessary to substantiate the results reported here. In particular, it is our intention to do future experiments for various storm surge events considering three dimensional storm surge processes and the effects of waves on the bottom stress, which were not included in this study.

Acknowledgements

This work was supported by the Korea Meteorological Administration Research and Development Program under CATER 2006-2301.

References

Alamaro, M., K. Emanuel, J. Colton, W. McGillis, Edson, J.B. 2002. Experimental investigation of air–sea transfer of momentum and enthalpy at high wind speed, Preprints, 25th Conference on Hurricanes and Tropical Meteorology, San Diego, CA, Am. Meteor. Soc., pp. 667–668.

Cardone, V.J., Cox, A.T., Greenwood, J.A., Thompson, E.F. 1994. Upgrade of Tropical Cyclone Surface Wind Field Model. CERC-94-14, US Army Corps of Engineers, pp. 102.

Charnock, H., 1955. Wind stress on a water surface. Quart. J. Roy. Meteor. Soc. 81, 639–640.

Donelan, M.A., 1990. Air–sea interaction. In: le Mehaute, B., Hanes, D.M. (Eds.), The Sea: Ocean Engineering Science, vol. 9B. Wiley-INTERSCIENCE, New York, pp. 239–292.

Donelan, M.A., Haus, B.K., Reul, N., Plant, W.J., Stiassnie, M., Graber, H.C., Brown, O.B., Saltzman, E.S., 2004. On the limiting aerodynamic roughness of the ocean in very strong winds. Geophys. Res. Lett. 31, L18306.

Doyle, J.D., 2002. Coupled atmosphere–ocean wave simulations under high wind conditions. Mon. Wea. Rev. 130, 3087–3099.

Drennan, W.M., Graber, G.C., Hauser, D., Quentin, C., 2003. On the wave age dependence of wind stress over pure wind seas, J. Geophys. Res. 108 (C3), 8062. doi:10.1029/2000JC000715.

Emanuel, K.A., 2003. A similarity hypothesis for air–sea exchange at extreme wind speeds. J Atmos. Sci. 60, 1420–1428.

Hara, T., Belcher, S.E., 2002. Wind forcing in the equilibrium range of wind-wave spectra. J. Fluid Mech. 470, 223–245.

Hara, T., Belcher, S.E., 2004. Wind profile and drag coefficient over mature ocean surface wave spectra. J. Phys. Oceanogr. 34, 2345–2358.

Janssen, P.A.E.M., 1989. Wave induced stress and the drag of air flow over sea waves. J. Phys. Oceanogr. 19, 745–754.

Janssen, P.A.E.M., 1991. Quasi-linear theory of wind-wave generation applied to wave forecasting. J. Phys. Oceanogr. 21, 1631–1642.

Janssen, P.A.E.M., 1992. Experimental evidence of the effect of surface waves on the airflow. J. Phys. Oceanogr. 22, 1600–1604.

JTWC, 2003. Annual tropical cyclone report. Available from: <http://metocph.nmci.navy.mil/jtwc.php>.

Kang, S.-W., Jun, K.-C., Park, K.-S., Bang, G.-H., 2002. A comparison of typhoon wind models with observed winds. J. Korean Soc. Oceanogr. 7, 100–107 (In Korean with English abstract).

Kim, K.O., Yamashita, T., Choi, B.H., 2008. Coupled process-based cyclone surge simulation for the Bay of Bengal. Ocean Modell. 25, 132–143.

Kwon, J.-I., Lee, J.-C., Park, K.-S., Jun, K.-C., 2008. Comparison of typhoon wind models based on storm surge heights induced by Typhoon Maemi. Asia–Pacific J. Atmos. Sci. 44, 443–454.

Large, W.G., Pond, S., 1981. Open ocean momentum flux measurements in moderate to strong wind. J. Phys. Oceanogr. 11, 324–336.

Lee, J.-C., Kwon, J.-I., Park, K.-S., Jun, K.-C., 2008. Calculations of storm surges, Typhoon Maemi. J. Korean Soc. Coastal Ocean Eng. 20, 93–100.

Mastenbroek, C., Burgers, G., Janssen, P.A.E.M., 1993. The dynamical coupling of a wave model and a storm surge model through the atmospheric boundary layer. J. Phys. Oceanogr. 23, 1856–1866.

Monin, A.S., Obukhov, A.M., 1954. Basic laws of turbulent mixing in the surface layer of the atmosphere. Tr Geofiz. Inst. Akad. Navk SSSR 24, 163–187.

Moon, I.-J., 2005. Impact of a coupled ocean wave-tide-circulation system on coastal modeling. Ocean Modell. 8 (3), 203–236.

Moon, I.-J., Ginis, I., Hara, T., Tolman, H., Wright, C.W., Walsh, E.J., 2003a. Numerical simulation of sea-surface directional wave spectra under hurricane wind forcing. J. Phys. Oceanogr. 33, 1680–1706.

Moon, I.-J., Oh, I.S., Murty, T., Youn, Y.-H., 2003b. Causes of unusual coastal flooding generated by Typhoon Winnie on the west coast of Korea. Natural Hazards 29, 485–500.

Moon, I.-J., Hara, T., Ginis, I., Belcher, S.E., Tolman, H., 2004a. Effect of surface waves on air–sea momentum exchange. Part I: Effect of mature and growing seas. J Atmos. Sci. 61, 2321–2333.

Moon, I.-J., Ginis, I., Hara, T., 2004b. Effect of surface waves on air–sea momentum exchange. II: Behavior of drag coefficient under tropical cyclones. J Atmos. Sci. 61, 2334–2348.

Moon, I.-J., Ginis, I., Hara, T., 2004c. Effect of surface waves on Charnock coefficient under tropical cyclones. Geophys. Res. Lett. 31, L20302.

Moon, I.-J., Ginis, I., Hara, T., 2008. Impact of the reduced drag coefficient on ocean wave modeling under hurricane conditions. Mon. Wea. Rev. 136, 1217–1223.

Moon, I.-J., Ginis, I., Hara, T., Thomas, B., 2007. A Physics-based parameterization of air–sea momentum flux at high wind speeds and its impact on hurricane intensity predictions. Mon. Wea. Rev. 135, 2869–2878.

Moon, I.-J., Oh, I.S., 2003. A study of the effect of waves and tides on storm surge using a coupled ocean wave-circulation model. J. Korean Meteorol. Soc. 39 (5), 563–574.

Powell, M.D., Vickery, P.J., Reinhold, T.A., 2003. Reduced drag coefficient for high wind speeds in tropical cyclones. Nature 422, 279–283.

Smith, S.D., Anderson, R.J., Oost, W.A., Kraan, C., Maat, N., DeCosmo, J., Katsaros, K.B., Davidson, K.L., Bumke, K., Hasse, L., Chadwick, H.M., 1992. Sea surface wind stress and drag coefficients: The HEXOS results. Bound. Layer Meteor. 60, 109–142.

Stelling, G.S., 1984. On the construction of computational methods for shallow water flow problems. Rijkswaterstaat Communications, 35, The Hague, Rijkswaterstaat, pp. 230.

Strikwerda, J.C., 1989. Finite Difference Schemes and Partial Difference Equations, Wadsworth, Inc. Belmount, Calif. pp. 101.

Tolman, H.L., 2002. User manual and system documentation of WAVEWATCH-III version 2.22. NOAA/NWS/NCEP/OMB Technical Note 222, pp. 133.

Tolman, H.L., Alves, J.H.G.M., Chao, Y.Y., 2005. Operational forecasting of wind-generated waves by hurricane Isabel at NCEP. Wea Forecasting 20, 544–557.

Tolman, H.L., Chalikov, D., 1996. Source terms in a third-generation wind-wave model. J. Phys. Oceanogr. 26, 2497–2518.

Wu, J., 1982. Wind-stress coefficients over sea surface from breeze to hurricane. J. Geophys. Res. 87, 9704–9706.

Xie, L., Liu, H., Peng, M., 2008. The effect of wave–current interactions on the storm surge and inundation in Charleston Harbor during Hurricane Hugo 1989. Ocean Modell. 20 (3), 252–269.

Zhang, M.Y., Li, Y.S., 1997. The dynamic coupling of a 3rd-generation wave model and a 3d hydrodynamic model through boundary-layers. Cont. Shelf Res. 17, 1141–1170.